Hindawi
Shock and Vibration
Volume 2017, Article ID 2104015, 17 pages
https://doi.org/10.1155/2017/2104015

Research Article

Effects of Transverse Deformation on Free Vibration of 2D Curved Beams with General Restraints

Xueren Wang,[1] Xuhong Miao,[1,2] Di Jia,[1] and Shengyao Gao[1]

[1] *Naval Academy of Armament, Beijing 100161, China*
[2] *College of Shipbuilding Engineering, Harbin Engineering University, Harbin 150001, China*

Correspondence should be addressed to Xueren Wang; wangxuerennaa@126.com

Received 1 July 2017; Revised 1 September 2017; Accepted 11 September 2017; Published 18 October 2017

Academic Editor: Nerio Tullini

An efficient modified Fourier series-based sampling surface approach is proposed for the analytical evaluation of the vibration characteristics of thick curved beams subjected to general restraints. The theoretical models of the beams are formulated by the theory of elasticity in two dimensions, which allows arbitrary thickness configurations to be tackled. As an innovation of this work, the approach is based upon the sampling surface method combined with the use of modified Fourier series approximation. In particular, the transverse beam domain is discretized by a set of sampling surfaces with unequal spaces, and the displacement components in beam domain coinciding with these surfaces are mathematically described as a set of modified Fourier series in which certain supplementary functions are included to remove all the relevant discontinuities with the displacements and their derivatives at the boundaries to form a mathematically complete set and guarantee the results convergent to the exact solutions. The final results are numerically solved using a modified variational principle by means of Lagrange multipliers and penalty method for the sake of arbitrary boundary conditions. The influences of transverse normal and shear deformation on the vibration characteristics with respect to the geometrical dimension and boundary conditions are systematically evaluated.

1. Introduction

Beams are one of the most extensively used structural components in a variety of branches of engineering applications, such as aircraft, civil construction, automobile, and naval vessel. The analytical evaluation of the vibration characteristics of beams has attracted much attention in the past decades because this information is very important for the low-vibration design and safety validation of engineering structures.

Strictly speaking, beams are three-dimensional (3D) blocks in physical sense for which the axial length is relatively larger than the other two dimensions. The 3D linear theory of elasticity may be applied in the theoretical modeling. However, such studies require high computing performance and lager storage capacities [1]. As a consequence, the beam problems are always simplified to a variety of one-dimensional (1D) representations by introducing several hypotheses in the kinetic relations and constitutive equations since the axial dimensions are relatively larger than the others. A variety of simplified 1D theories have been proposed so far, which are commonly divided into two aspects as follows: the classical beam theory (CBT) and the shear deformation beam theories (SDBTs). These specialties make them very attractive in the mechanics analysis of beams [2–10]. However, it is needed to be pointed out that the CBT is incapable of considering transverse deformation effect. The error of the calculating result is always great when dealing with moderately thick beams [11], since the shear effects on the cross section are more pronounced in moderately thick to thick beams and they are disregarded in the CBT. The FSDT overcomes this drawback and offers a more accuracy modeling theory since transverse deformation is further taken into account, even though the solutions based on the FSDTs are still not accurate due to the fact that the transverse normal components are still neglected. In addition, shear correction factors have to be incorporated in the FSDTs to adjust the transverse shear stiffness due to the fact that the transverse shear strains in the FSDTs are assumed to be constant in the thickness direction. The shear correction factors are difficult to determine because they depend not only on the geometric parameters, but also on the loading and boundary conditions. In order to obtain accurate solutions for thick beams, higher-order variation of axial displacement has been introduced into a wide variety of HSDTs. These theories are more accurate than the CBT and FSDTs without shear correction factors. But, unfortunately, the transverse normal effects are ignored in the conventional HSDTs. Thus, in order to analyze thick beams accurately, more advanced theories considering the through-thickness shear deformations are essentially required. Recently, Carrera [12, 13] developed the so-called Carrera Unified Formulation (CUF). According to the CUF, the obtained theories can have an order of expansion depending on the thickness functions that are used, which allows one to take into account the effects of the transverse normal effects.

The static and dynamic analysis of thick beam has been extensively investigated by many researchers. Chen et al. [14] proposed a mixed approach for the bending and free vibration of arbitrarily thick beams. In their method, the state space method and the differential quadrature method are combined to solve the problems. The method was further applied to the calculation of the elasticity solution of FGM beams by Ying et al. [15]. Hasheminejad and Rafsanjani [16] obtained semianalytical results for the transient dynamic response of thick simply supported beams through a powerful state space technique and the Laplace transformation. Thermoelastic behavior of arbitrarily simply supported beams subjected to thermomechanical loads is studied by Xu and Zhou [17, 18]. Zenkour et al. [19] studied the influence of transverse deformations on fiber reinforced viscoelastic beams. Malekzadeha and Karami [20] developed a mixed differential quadrature (DQ) and finite element (FE) approach for free vibration and buckling analysis of thick beams. This method applies a finite element discretization technique along axial direction while the thickness direction is discretized using DQM. The developments of studies of static and dynamic analysis of beams can be found in several monographs by Qatu [1], Rosen [21], Chidamparam and Leissa [22], Hodges [23], and Hajianmaleki and Qatu [24].

From the review of the literature, it is clear that although a lot of attention has been focused on static and dynamic analysis of thick beams, the extensive volume of literature on this subject was mainly limited to uniform straight beams with classical boundary conditions since their governing equation is much easier to be derived and tackled. The equations for a curved beam are more complicate and sophisticated because of curvilinear geometry. Inevitably, this introduces inherent complexity in finding their solutions [25]. In addition, the previous reviews showed that most beams are analyzed based on Euler-Bernoulli beam theory, Timoshenko beam theory, or the higher-order one-dimensional theory models which neglect the transverse normal deformation effect (thickness stretching). This appears quite inappropriate since the effect of transverse normal deformation on the static dynamic characteristics of thick beams is significant, especially at higher vibration modes of curved beams. Carrera et al. [26] and Koiter [27] recommended that a refinement of one-dimensional simplification theories is meaningless, unless the effects of transverse shear and normal deformations are all taken into account. Thus, seldom works are available that investigate the influences of transverse shear and normal deformations on the vibration characteristics of evident thick curved beams. The present work attempts to fill this gap.

In this paper, the modified Fourier series-based sampling surface method is further extended to the evaluation of elasticity solution of thick curved beams. The method was developed by Ye and Jin [28] based on a modified Fourier series technique proposed by Li [29] and SaS approach originally proposed by Kulikov et al. [30, 31]. The method combines the advantages of both approaches. A comprehensive numerical analysis and discussions are conducted to investigate the influence of transverse normal and shear deformations on the vibration characteristics of curved beams. The article is organized as follows: the theoretical formulation including model description, plan stress assumption, application of sampling surface method, and modified Fourier series approximation is presented in Section 2; convergence studies, results verification, and transverse deformation investigation are given in Section 3 and the concluding remarks are summarized in Section 4.

2. Theoretical Formulations

2.1. Model Description. A thick circular beam shown in Figure 1 is considered, in which b, h, and R represent the width, thickness, and inner radius of the beam. The beam is bounded along its edges by the boundaries $\theta = \theta_0$ and $\theta = \theta_1$. The bottom surface of the beam is selected as the reference surface with the three orthogonal curvilinear coordinates θ, y, and z; see Figure 1. In this paper, the beams are assumed to be isotropic and homogeneous and to vibrate freely in the θ-z plane. u, v, and w denote the three displacement components in the axial, lateral, and normal directions, respectively.

2.2. Plane Stress Assumption. As mentioned previously, the beam under consideration vibrates freely in the θ-z plane. Therefore, the plane stress hypothesis is adopted in the theoretical formulation for the purpose of improving the computational efficiency and maintaining the modeling precision synchronously.

For a curved beam, the 3D strain-displacement relations for any point in the domain of the beam can be found as [32]

$$\begin{aligned}
\varepsilon_\theta &= \frac{1}{R_z}\left(\frac{\partial u}{\partial \theta} + w\right),\\
\gamma_{\theta z} &= \frac{\partial u}{\partial z} + \frac{1}{R_z}\left(\frac{\partial w}{\partial \theta} - u\right),\\
\varepsilon_y &= \frac{\partial v}{\partial y},\\
\gamma_{yz} &= \frac{\partial v}{\partial z} + \frac{\partial w}{\partial y},\\
\varepsilon_z &= \frac{\partial w}{\partial z},\\
\gamma_{\theta y} &= \frac{\partial u}{\partial y} + \frac{1}{R_z}\left(\frac{\partial v}{\partial \theta}\right),
\end{aligned} \tag{1}$$

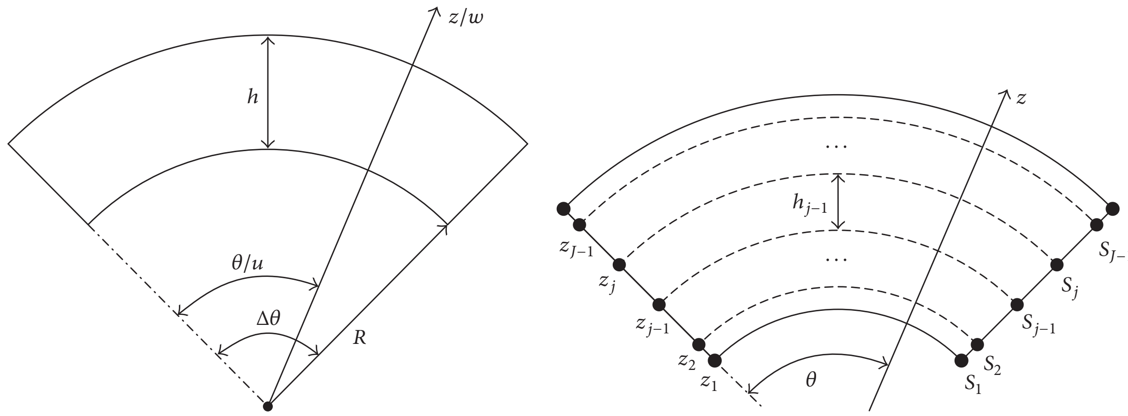

(a) Coordinate system (b) Sampling surface distribution

Figure 1: Geometry and reference system for a curved beam and the diagrammatic sketch of sampling surface distribution.

where $R_z = R + z$, ε_θ, ε_y, and ε_z stand for the normal strains, and γ_{yz}, $\gamma_{\theta z}$, and $\gamma_{\theta y}$ are the shear components. In the case of homogeneous materials and linear small deformation assumptions, the 3D stresses can be derived according to Hooke's law:

$$\begin{Bmatrix} \sigma_\theta \\ \sigma_y \\ \sigma_z \\ \tau_{yz} \\ \tau_{\theta z} \\ \tau_{\theta y} \end{Bmatrix} = \begin{bmatrix} C'_{11} & C'_{12} & C'_{13} & 0 & 0 & 0 \\ C'_{12} & C'_{22} & C'_{23} & 0 & 0 & 0 \\ C'_{13} & C'_{23} & C'_{33} & 0 & 0 & 0 \\ 0 & 0 & 0 & C'_{44} & 0 & 0 \\ 0 & 0 & 0 & 0 & C'_{55} & 0 \\ 0 & 0 & 0 & 0 & 0 & C'_{66} \end{bmatrix} \begin{Bmatrix} \varepsilon_\theta \\ \varepsilon_y \\ \varepsilon_z \\ \gamma_{yz} \\ \gamma_{\theta z} \\ \gamma_{\theta y} \end{Bmatrix} = \mathbf{C}'\boldsymbol{\varepsilon}, \quad (2)$$

where σ_θ, σ_y, and σ_z stand for the normal stresses; τ_{yz}, $\tau_{\theta z}$, and $\tau_{\theta y}$ are the shear component. $\mathbf{C}'$ is the material stiffness matrix.

$$\begin{aligned} C'_{11} &= C'_{22} = C'_{23} = \frac{E(1-\nu)}{(1+\nu)(1-2\nu)}, \\ C'_{12} &= C'_{13} = C'_{23} = \frac{\nu C'_{11}}{(1-\nu)}, \\ C'_{44} &= C'_{55} = C'_{66} = \frac{E}{2(1+\nu)} \end{aligned} \quad (3)$$

in which E means Young's module of the material and ν represents Poisson's ratio.

Furthermore, (2) can be rearranged in the form of matrix as

$$\begin{aligned} \begin{Bmatrix} \boldsymbol{\sigma}_i \\ \boldsymbol{\sigma}_o \end{Bmatrix} &= \begin{bmatrix} \mathbf{C}'_{ii} & \mathbf{C}'_{io} \\ \mathbf{C}'_{oi} & \mathbf{C}'_{oo} \end{bmatrix} \begin{Bmatrix} \boldsymbol{\varepsilon}_i \\ \boldsymbol{\varepsilon}_o \end{Bmatrix}, \\ \boldsymbol{\sigma}_i &= \begin{Bmatrix} \sigma_\theta \\ \sigma_z \\ \tau_{\theta z} \end{Bmatrix}, \\ \boldsymbol{\sigma}_o &= \begin{Bmatrix} \sigma_y \\ \tau_{yz} \\ \tau_{\theta y} \end{Bmatrix}, \\ \boldsymbol{\varepsilon}_i &= \begin{Bmatrix} \varepsilon_\theta \\ \varepsilon_z \\ \gamma_{\theta z} \end{Bmatrix}, \\ \boldsymbol{\varepsilon}_o &= \begin{Bmatrix} \varepsilon_y \\ \gamma_{yz} \\ \gamma_{\theta y} \end{Bmatrix}, \\ \mathbf{C}'_{ii} &= \begin{bmatrix} C'_{11} & C'_{13} & 0 \\ C'_{13} & C'_{33} & 0 \\ 0 & 0 & C'_{55} \end{bmatrix}, \\ \mathbf{C}'_{io} &= \begin{bmatrix} C'_{12} & 0 & 0 \\ C'_{23} & 0 & 0 \\ 0 & 0 & 0 \end{bmatrix} = \left(\mathbf{C}'_{oi}\right)^{\mathrm{T}}, \\ \mathbf{C}'_{oo} &= \begin{bmatrix} C'_{22} & 0 & 0 \\ 0 & C'_{44} & 0 \\ 0 & 0 & C'_{66} \end{bmatrix}. \end{aligned} \quad (4)$$

Therefore, the final stress-strain relations for the beam under plane stress hypothesis can be obtained as

$$\boldsymbol{\sigma}_i = \mathbf{C}\boldsymbol{\varepsilon}_i, \quad (5)$$

where $\mathbf{C} = \mathbf{C}'_{ii} - \mathbf{C}'_{io}(\mathbf{C}'_{oo})^{-1}\mathbf{C}'_{io}$.

2.3. Application of Sampling Surface Technique. The sampling surface technique was originally proposed by Kulikov et al. [33–35]. A brief resume and application of this technique are included in this section.

As shown in Figure 1, $S_1, \ldots, S_j, \ldots, S_J$ stand for the chosen sampling surfaces inside the transverse domain of the beam to introduce the displacement components of these surfaces as basic beam variables. J is the total number of the sampling surfaces. These surfaces are selected to be nonequally spaced and paralleled to the beam's middle surface. For application of the sampling surface technique, it was found that the distribution of the sampling surface has a great effect on the convergence and accuracy of the solutions. For the sake of the convergence, transverse coordinates of these surfaces are chosen as the roots of Chebyshev polynomial:

$$\begin{aligned} z_1 &= 0, \\ z_J &= h, \\ z_j &= \frac{z_1 + z_J}{2} - \frac{h}{2}\cos\left(\pi\frac{2j-3}{2J-4}\right); \\ &\qquad 2 \le j \le J-1. \end{aligned} \tag{6}$$

Therefore, the basic variables in the axial and normal directions of an arbitrary sampling surface can be given by

$$\begin{aligned} u\left(\theta, z_j, t\right) &= u_j(\theta)\, e^{i\omega t}, \\ w\left(\theta, z_j, t\right) &= w_j(\theta)\, e^{i\omega t}; \\ &\qquad 1 \le j \le J, \end{aligned} \tag{7}$$

where $u_j(\theta)$ and $w_j(\theta)$ stand for the axial and transverse displacement components, respectively. t stand for the time variable, ω is the circular frequency. As a consequence, displacement field of the beam under vibration can be calculated by

$$\begin{aligned} &\{u(\theta, z, t), w(\theta, z, t)\} \\ &\quad = \sum_j \left\{L_j(z)\, u_j(\theta), L_j(z)\, w_j(\theta)\right\} e^{i\omega t}; \\ &\qquad z_1 \le z \le z_J \end{aligned} \tag{8}$$

and $L_j(z)$ is Lagrange's interpolation of degree $J-1$:

$$L_j(z) = \prod_{r \ne j} \frac{z - z_r}{z_j - z_r}; \quad z_1 \le z \le z_J. \tag{9}$$

According to (1), strains on the jth sampling surface can be found as

$$\begin{aligned} &\left\{\varepsilon_\theta\left(\theta, z_j, t\right), \varepsilon_z\left(\theta, z_j, t\right), \gamma_{\theta z}\left(\theta, z_j, t\right)\right\} \\ &\quad = \left\{\varepsilon_\theta^j(\theta), \varepsilon_z^j(\theta), \gamma_{\theta z}^j(\theta)\right\} e^{i\omega t}; \quad 1 \le j \le J, \\ &\varepsilon_\theta^j(\theta) = \frac{1}{R + z_j}\left(\frac{\partial u_j(\theta)}{\partial\theta} + w_j(\theta)\right), \\ &\varepsilon_z^j(\theta) = \sum_r M_j^r w_r(\theta), \\ &\gamma_{\theta z}^j(\theta) = \sum_r M_j^r u_r(\theta) + \frac{1}{R + z_j}\left(\frac{\partial w_j(\theta)}{\partial\theta} - u_j(\theta)\right), \end{aligned} \tag{10}$$

where M_j^r are determined by

$$\begin{aligned} M_j^r &= \frac{1}{z_r - z_j}\prod_{s \ne r, j}\frac{z_j - z_s}{z_r - z_s} \quad \text{for } r \ne j, \\ M_j^j &= -\sum_{r \ne j} M_j^r \quad \text{for } r = j. \end{aligned} \tag{11}$$

Similarly, strain distribution in the whole space should be represented as a linear combination of their corresponding strain components of the entire sampling surfaces as (8).

$$\begin{aligned} &\{\varepsilon_\theta, \varepsilon_z, \gamma_{\theta z}\} \\ &\quad = \sum_j \left\{L_j(z)\,\varepsilon_\theta^j(\theta), L_j(z)\,\varepsilon_z^j(\theta), L_j(z)\,\gamma_{\theta z}^j(\theta)\right\} e^{i\omega t}; \\ &\qquad z_1 \le z \le z_J. \end{aligned} \tag{12}$$

The energy functional for the curved beam under the circumstance of free vibration is

$$\Pi_s = T_s - U_s, \tag{13}$$

where U_s and T_s denote the strain and kinetic energy function defined as follows:

$$\begin{aligned} U_s &= \frac{1}{2}\iint_S \int_{z_1}^{z_J} \{\sigma_\theta\varepsilon_\theta + \sigma_z\varepsilon_z + \tau_{\theta z}\gamma_{\theta z}\}(R + z)\, d\theta\, dy\, dz, \\ T_s &= \frac{1}{2}\iint_S \int_{z_1}^{z_J} \rho\left\{u_{,t}^2 + w_{,t}^2\right\}(R + z)\, d\theta\, dy\, dz, \end{aligned} \tag{14}$$

where ρ stands for the material density. Substituting (5) and (12) into (14), the two energy functions can be further written as

$$\begin{aligned} U_s = \frac{1}{2}\iint_S \int_{\zeta_1}^{\zeta_J} \Bigg\{ & C_{11}\left(\sum_i\sum_j \frac{L_i L_j}{R_i R_j}\frac{\partial u_i}{\partial\theta}\frac{\partial u_j}{\partial\theta} + 2\sum_i\sum_j \frac{L_i L_j}{R_i R_j}\frac{\partial u_i}{\partial\theta} w_j + \sum_i\sum_j \frac{L_i L_j}{R_i R_j} w_i w_j\right) + 2C_{12}\sum_{i,r}\sum_j M_r^i \frac{L_r L_j}{R_j} w_i \frac{\partial u_j}{\partial\theta} \\ & + 2C_{12}\sum_{i,r}\sum_j M_r^i \frac{L_r L_j}{R_j} w_i w_j + C_{22}\sum_{i,s}\sum_{j,r} M_s^i M_r^j L_s L_j w_i w_j + C_{33}\sum_{i,s}\sum_{j,r} M_s^i M_r^j L_s L_j u_i u_j + C_{33}\sum_{i,s}\sum_j M_s^i \frac{L_s L_j}{R_j} u_i \frac{\partial w_j}{\partial\theta} \end{aligned}$$

$$
\begin{aligned}
&- 2C_{33}\sum_{i,s}\sum_{j} M_s^i \frac{L_s L_j}{R_j} u_i u_j + C_{33}\sum_{i}\sum_{j,r} M_r^j \frac{L_i L_r}{R_i}\frac{\partial w_i}{\partial \theta} u_j + C_{33}\sum_{i}\sum_{j}\frac{L_i L_j}{R_i R_j}\frac{\partial w_i}{\partial \theta}\frac{\partial w_j}{\partial \theta} - 2C_{33}\sum_{i}\sum_{j}\frac{L_i L_j}{R_i R_j}\frac{\partial w_i}{\partial \theta} u_j \\
&\left. + C_{33}\sum_{i}\sum_{j}\frac{L_i L_j}{R_i R_j} u_i u_j \right\} R_z d\theta\, dy\, dz, \\
&T_s = \frac{1}{2}\iint_S \int_{\zeta_1}^{\zeta_J} -\rho\omega^2 \left\{ \sum_i\sum_j L_i L_j u_i u_j + \sum_i\sum_j L_i L_j w_i w_j \right\} R_z d\theta\, dy\, dz.
\end{aligned}
\tag{15}
$$

2.4. Modified Fourier Series Approximation. The modified Fourier series approximation is introduced to represent the possible deformations of the curved beams. Particularly, each of the basic beam variables is mathematically described as a set of modified Fourier series including a standard cosine Fourier series as well as certain auxiliary functions [36–41]. The auxiliary terms are introduced for the purpose of removing the entire possible discontinuities with the basic beam variables and their derivatives at the edges to form a mathematically complete set and then ensure the convergence and speed up the calculation [39, 42–45]. In addition, the governing equations of the beams are derived and numerically solved by a modified variational principle for the sake of making arbitrary boundary conditions applicable.

As mentioned previously, the displacement variables at an arbitrary sampling surface in the modified form of Fourier series are

$$
\begin{aligned}
u_j(\theta) &= \sum_{n=0}^{N-2} u_j^n \cos\left(\frac{n\pi\theta}{\Delta\theta}\right) + u_j^{N-1}\theta\left(\frac{\theta}{\Delta\theta - 1}\right)^2 \\
&\quad + u_j^N \theta^2 \frac{(\theta/\Delta\theta - 1)}{\Delta\theta}, \\
w_j(\theta) &= \sum_{n=0}^{N-2} w_j^n \cos\left(\frac{n\pi\theta}{\Delta\theta}\right) + w_j^{N-1}\theta\left(\frac{\theta}{\Delta\theta - 1}\right)^2 \\
&\quad + w_j^N \theta^2 \frac{(\theta/\Delta\theta - 1)}{\Delta\theta},
\end{aligned}
\tag{16}
$$

where u_j^n and $w_j^n (n = 0, 1, \ldots, N)$ are the expansion coefficients; $\Delta\theta = \theta_1 - \theta_0$. N represents the truncation number.

The boundary conditions of the curved beams are supposed to be of essential type. The necessary boundary equations can be stated in functional form as follows by applying the penalty technique and Lagrange multipliers [6, 46–49]:

$$
\begin{aligned}
&\Pi_b = \Pi_{b1} + \Pi_{b2}; \\
&\Pi_{b1} \\
&= \int\int_{z_1}^{z_J}\sum_{l=1}^{2}(-1)^l \left\{\eta_u^l \sigma_\theta \left(u - \overline{u}^l\right) + \eta_w^l \tau_{\theta z}\left(w - \overline{w}^l\right)\right\}\Big|_{\theta=\theta_l} dy\, dz, \\
&\Pi_{b2} \\
&= \frac{1}{2}\int\int_{z_1}^{z_J}\sum_{l=1}^{2}\left\{\eta_u^l k_u^l \left(u - \overline{u}^l\right)^2 + \eta_u^l k_w^l \left(w - \overline{w}^l\right)^2\right\}\Big|_{\theta=\theta_l} dy\, dz,
\end{aligned}
\tag{17}
$$

where $\overline{u}^l$ and $\overline{w}^l$ denote the boundary values. k_u^l and k_w^l represent the penalty parameters. η_u^l and η_w^l are the parameters which define different restraint conditions. The boundary potential Π_{b1} is introduced by means of Lagrange multiplier technique while the boundary potential Π_{b2} is introduced by the aid of the penalty technique to ensure a uniform formulation to tackle general boundaries [6] and to ensure a computational stability in computational process. Taking the end of $\theta = \theta_0$, for example, the values of the penalty parameters and boundary coefficients for different classical restraint conditions are shown in Table 1. For elastic boundary conditions, the boundary potentials Π_{b1} in (17) should be neglected and the penalty parameters will be determined at proper values [49].

Therefore, the final variational functional for the curved beam with general boundaries is defined as

$$
\Pi_{\text{total}}\left(u_j^n, w_j^n\right) = \Pi_s + \Pi_b; \quad 0 \le n \le N, \; 1 \le j \le J. \tag{18}
$$

Finally, let the variation of the Π_{total} with respect to each coefficient (u_j^n and w_j^n) equal zero; the governing equations can be derived in a matrix form as

$$
\left\{\mathbf{K} - \omega^2\mathbf{M}\right\}\mathbf{G} = \mathbf{0}, \tag{19}
$$

where $\mathbf{K}$ and $\mathbf{M}$ stand for the final stiffness and mass matrices of order $2(N + 1) * J$. $\mathbf{G}$ denotes the vector of the unknown generalized displacements. Thus, solutions can be obtained directly by the eigenvalue decomposition of (19) and the roots of the decomposition are the square of eigenfrequency ω. The mode shape of the curved beam corresponding to each eigenfrequency can be constructed by substituting the corresponding eigenvector back into the displacement variables given in (16) and then substituting it in the displacement distribution formula given in (8).

Table 1: Values of η_u^l, η_w^l, k_u^l, and k_w^l for different classical boundary conditions.

Boundary conditions	Boundary coefficients		Penalty parameters	
	η_u^0	η_w^0	k_u^0	k_w^0
F (free): $\sigma_\theta = 0$, $\tau_{\theta z} = 0$	0	0	0	0
S1 (simply supported): $\sigma_\theta = 0$, $w = 0$	0	1	0	$10^3 E$
S2 (simply supported): $u = 0$, $\tau_{\theta z} = 0$	1	0	$10^3 E$	0
C (clamped): $u = 0$, $w = 0$	1	1	$10^3 E$	$10^3 E$

3. Numerical Results and Discussion

Several examples for thick curved beams with different geometrical dimensions and boundary restraints are presented to verify the flexibility of the method. The transverse deformation effects are systematically investigated as well. To unify the discussion, character string X-Y (X/Y = F, S, C) is used to represent the boundary conditions of the beams. For example, C-F represents a circular beam with clamped and free restraints at the ends $\theta = \theta_0$ and $\theta = \theta_1$, respectively. To unify the discussion, the dimensionless variable of frequency is introduced in the calculation $\Omega = \omega R_m^2 \sqrt{12\rho/Eh^2}$ (where $R_m = R + h/2$). The beams are supposed to be made of steel ($E = 210$ GPa, $\nu = 0.3$, and $\rho = 7800\,\mathrm{kg/m^3}$).

3.1. Validation. Table 2 gives the first five nondimensional frequency parameters Ω of C-C supported circular beams. The numbers of the sampling surfaces and serious truncation are increased from 11 to 17 and 3 to 9, respectively. The geometric parameters of the beam are $R_m = 1$ m, $\Delta\theta = 2\pi/3$. For completeness, two thickness-to-radius ratios (i.e., $h/R_m = 0.1$ and 0.2) corresponding to the moderately thick and thick beam configurations are considered in the study. As observed from Table 2, with the increase of truncated number, the natural frequencies tend to be constant values quickly. The maximum differences between the results based on the "11 × 3" and "17 × 9" computational schemes are less than 0.2%, which confirms the high convergence of the present method. The DQM results based on the FSDT [3] and the Ritz solutions with 2D elasticity theory [32] are also listed in the table. It is observed that the present solutions match well with those predicted by Malekzadeh et al. [3] and Jin et al. [32]. The slight differences between the three groups of results show the satisfied accuracy of the proposed approach. Table 3 compares the first six natural frequencies (Hz) of a circular beam with F-F, F-C, and C-C boundary conditions obtained by the current approach with those based on commercial FEM code. The results are calculated with the beam parameters $R_m = 1$ m, $h/R_m = 0.3$ and with "17 × 9" truncation scheme. Calculations based on FEM commercial software ANSYS (PLANE82, 0.025 m) are used as the benchmark solutions. In Table 3, it is obvious that the present method produces good results comparing with FEM.

3.2. Transverse Deformation Effects. The effects of transverse deformation on the vibration characteristics of curved beams are investigated in this section. In Figures 2–9, relative deviations between frequency parameters Ω calculated by the CBT/FSDT theory models [5] and the present 2D approach for circular beams with various different geometries and boundary conditions are considered. The "deviations (%)" between the results are defined as

$$\text{Deviations}\,(\%) = \frac{(\Omega_{\text{CBT/FSDT}} - \Omega_{\text{2-D}})}{\Omega_{\text{2-D}}} \times 100\%. \tag{20}$$

Figures 2–4 show the relative deviations of the 1st, 3rd, and 5th frequency parameters Ω for circular beams with different ratios of thickness-to-span length (h/L_θ). The beam is supposed to be of unit span length; that is, $L_\theta = R\Delta\theta = 1$. The ratio of h/L_θ is varied between 0.01 and 0.2. F-F, C-C, and F-C boundaries are considered in the study. The results obtained by the current method of "$N \times J = 17 \times 8$" truncation scheme are selected as benchmark. From the figures, we can see that there is a clear increment of frequency parameter for the larger thickness-to-span length ratio and the increment becomes more prominent for higher modes. The maximum difference can be as much as 35%. Furthermore, results on the basis of CBT are generally higher than those based on FSDT model and the 2D elasticity theory because the effects of shear deformations are more significant in thick beams. It is due to the fact that hypotheses in the CBT will introduce additional stiffness in the modeling in fact. This investigation shows that the CBT can be grossly error for the modeling of moderately thick and thick curved beams. In addition, it is obvious that the results based on the FSDT are more accurate than those of CBT since the effects of traverse deformation are included.

Figure 5 shows a similar study for clamped circular beams with various thickness-to-radius ratios and span angles. Geometrical dimensions used in the study are $R_m = 1$ m. "$N \times J = 17 \times 9$" displacement field is adopted for the 2D solutions in this study. As expected, the effects of transverse normal and shear deformations decrease as the span angle increases. The relative deviations between results based on the CBT model and the current 2D approach are also very big and the maximum difference can be as much as 50%. It can be observed that that the effects of the transverse normal and shear deformation varied with mode number and (span) length-to-radius ratio. Generally, lower (span) length-to-radius ratio values will lead to larger modeling deviation of vibration behavior since transverse effects are more significant for short beams.

Figures 6 and 7 consider the fundamental and fifth mode frequency parameters Ω of a circular beam based on the CBT and FSDT theory models, respectively. The thickness-to-span length ratio, h/L_θ, is varied from 0.01 to 0.2, corresponding to thin to thick beam configurations. Two boundary conditions, that is, F-F and C-C, are considered in the studies. The beam is supposed to be of unit span length and unit radius, that is, $L_\theta = 1$, $R_m = 1$ m. From the figures, we can see that the effects of the shear deformation increase generally as the thickness-to-span length ratio increases. When the thickness-to-span length ratio is equal to 0.1, the difference between the CBT

Table 2: Convergence of the lowest five frequency parameters Ω for C-C supported curved beams (R_m = 1 m, $\Delta\theta = 2\pi/3$).

N	J	$h/R_m = 0.1$					$h/R_m = 0.2$				
		1	2	3	4	5	1	2	3	4	5
11	3	12.067	21.555	35.782	40.788	63.430	10.959	14.434	24.614	28.932	38.069
	5	12.001	21.432	35.717	40.411	63.114	10.791	14.369	24.234	28.727	37.409
	7	11.998	21.428	35.716	40.401	63.104	10.788	14.368	24.231	28.724	37.403
	9	11.996	21.426	35.715	40.396	63.097	10.786	14.368	24.229	28.722	37.400
12	3	12.043	21.551	35.771	40.679	63.110	10.945	14.433	24.609	28.924	38.004
	5	11.984	21.421	35.706	40.300	62.772	10.781	14.367	24.224	28.714	37.338
	7	11.981	21.418	35.704	40.293	62.761	10.779	14.366	24.219	28.712	37.332
	9	11.980	21.416	35.703	40.288	62.754	10.778	14.366	24.217	28.711	37.330
13	3	12.042	21.531	35.759	40.668	63.069	10.943	14.432	24.596	28.921	37.993
	5	11.979	21.407	35.694	40.275	62.318	10.777	14.365	24.215	28.709	37.326
	7	11.976	21.405	35.693	40.268	62.308	10.774	14.365	24.211	28.705	37.317
	9	11.975	21.403	35.693	40.264	62.302	10.773	14.364	24.209	28.704	37.314
14	3	12.029	21.529	35.757	40.628	63.032	10.937	14.432	24.594	28.918	37.982
	5	11.969	21.401	35.692	40.250	62.260	10.772	14.365	24.212	28.705	37.316
	7	11.967	21.398	35.691	40.245	62.249	10.769	14.363	24.206	28.701	37.309
	9	11.966	21.397	35.690	40.241	62.243	10.769	14.363	24.205	28.701	37.307
15	3	12.027	21.518	35.752	40.625	62.966	10.936	14.431	24.588	28.918	37.981
	5	11.966	21.394	35.688	40.239	62.218	10.771	14.364	24.206	28.703	37.314
	7	11.964	21.392	35.687	40.233	62.210	10.767	14.363	24.201	28.698	37.304
	9	11.963	21.390	35.687	40.230	62.206	10.766	14.363	24.200	28.697	37.302
16	3	12.020	21.516	35.751	40.606	62.964	10.933	14.431	24.587	28.917	37.976
	5	11.960	21.390	35.686	40.226	62.208	10.767	14.363	24.205	28.700	37.308
	7	11.959	21.387	35.685	40.222	62.199	10.764	14.362	24.198	28.696	37.299
	9	11.958	21.386	35.685	40.219	62.195	10.763	14.362	24.197	28.695	37.298
17	3	12.019	21.510	35.749	40.603	62.943	10.933	14.431	24.585	28.916	37.976
	5	11.958	21.385	35.684	40.220	62.194	10.767	14.363	24.202	28.699	37.308
	7	11.957	21.384	35.683	40.214	62.187	10.763	14.362	24.196	28.694	37.297
	9	11.956	21.382	35.683	40.212	62.183	10.762	14.361	24.195	28.693	37.295
FSDT [3]		11.391	20.392	34.001	—	—	10.271	13.622	23.107	—	—
2D [32]		11.470	20.575	34.105	38.963	60.102	10.507	13.773	23.691	27.680	36.752

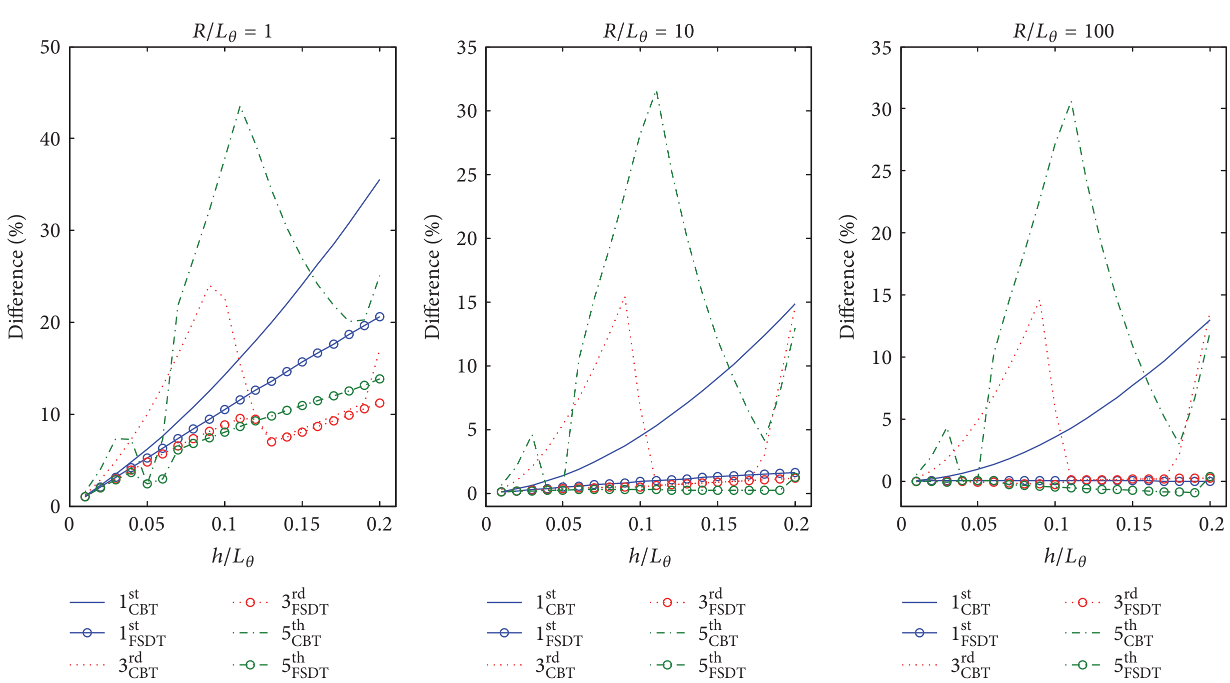

Figure 2: Relative deviations between the first, third, and fifth frequency parameters Ω based on the CBT/FSDT theory models to those of 2D theory for a complete free circular beam with various thickness ratios.

Table 3: The lowest six frequencies for circular beams with different boundary conditions, geometrical properties, and modeling methods (Hz, $R_m = 1$ m, $h/R_m = 0.3$).

BC	Mode	$\Delta\theta = \pi/4$ Pre.	FEM	Diff. (%)	$\Delta\theta = \pi/2$ Pre.	FEM	Diff. (%)	$\Delta\theta = 3\pi/4$ Pre.	FEM	Diff. (%)
F-F	1	1861.2	1861.3	0.003	545.85	545.85	0.001	239.19	239.19	0.000
	2	3304.8	3304.8	0.001	1333.9	1333.9	0.002	638.87	638.87	0.001
	3	3653.6	3653.9	0.007	1800.9	1800.9	0.001	1177.4	1177.4	0.001
	4	5514.5	5515.4	0.016	2285.0	2285.1	0.003	1355.5	1355.5	0.003
	5	5873.7	5874.5	0.014	3207.8	3207.9	0.004	1790.9	1790.9	0.002
	6	6166.1	6166.4	0.005	3344.4	3344.5	0.002	2289.5	2289.5	0.000
F-C	1	373.90	373.99	0.024	104.22	104.23	0.008	50.018	50.017	0.001
	2	1420.4	1420.6	0.014	431.29	431.32	0.008	182.16	182.15	0.003
	3	1870.6	1870.8	0.009	974.88	974.91	0.003	535.24	535.24	0.001
	4	3475.3	3475.8	0.013	1368.0	1368.1	0.005	898.42	898.43	0.001
	5	4773.6	4774.1	0.010	2131.7	2131.9	0.007	1173.9	1173.9	0.002
	6	5133.8	5134.0	0.005	2556.9	2556.9	0.001	1692.3	1692.3	0.002
C-C	1	1683.9	1684.5	0.033	850.21	850.24	0.004	512.94	512.93	0.002
	2	2923.8	2924.6	0.028	1079.5	1079.7	0.015	665.65	665.66	0.001
	3	3461.9	3462.8	0.027	1805.4	1805.5	0.007	1159.1	1159.1	0.002
	4	4991.2	4992.3	0.022	2056.6	2056.9	0.012	1227.9	1227.9	0.002
	5	6282.3	6283.3	0.017	2984.2	2984.5	0.009	1732.5	1732.5	0.002
	6	6414.4	6414.6	0.003	3280.8	3281.0	0.005	2148.3	2148.3	0.001

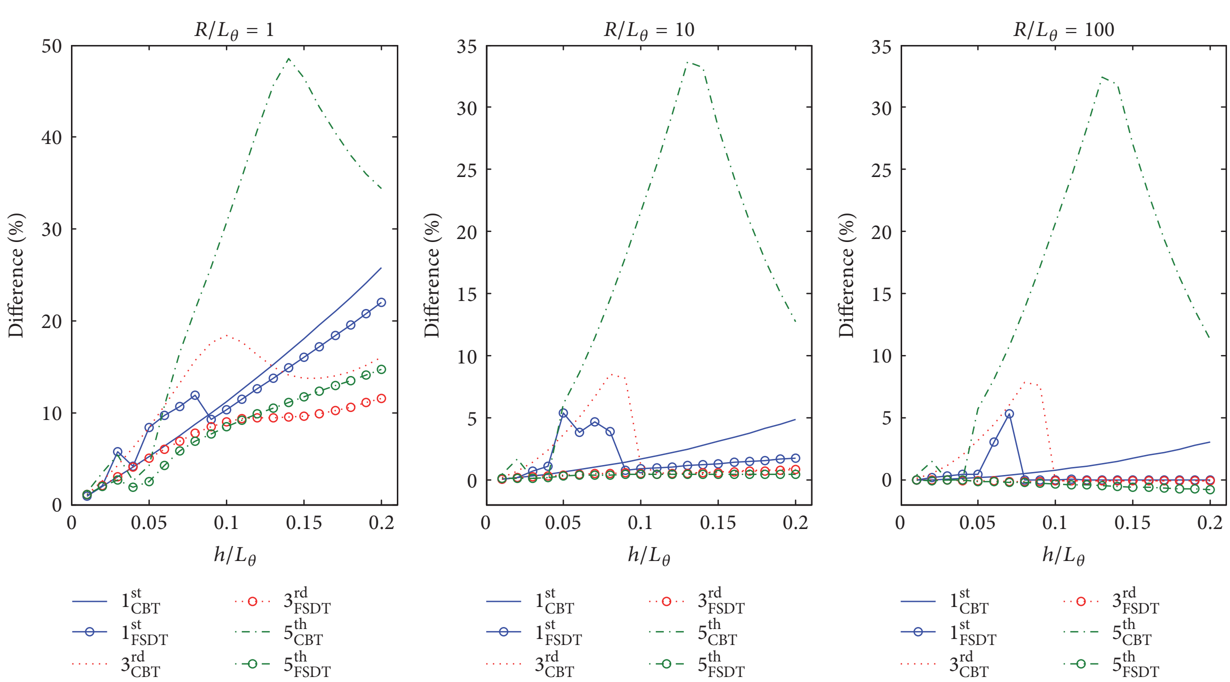

Figure 3: Relative deviations between frequency parameters Ω based on the CBT/FSDT theory models to those of 2D theory for circular beams with various thickness ratios (F-C boundary condition).

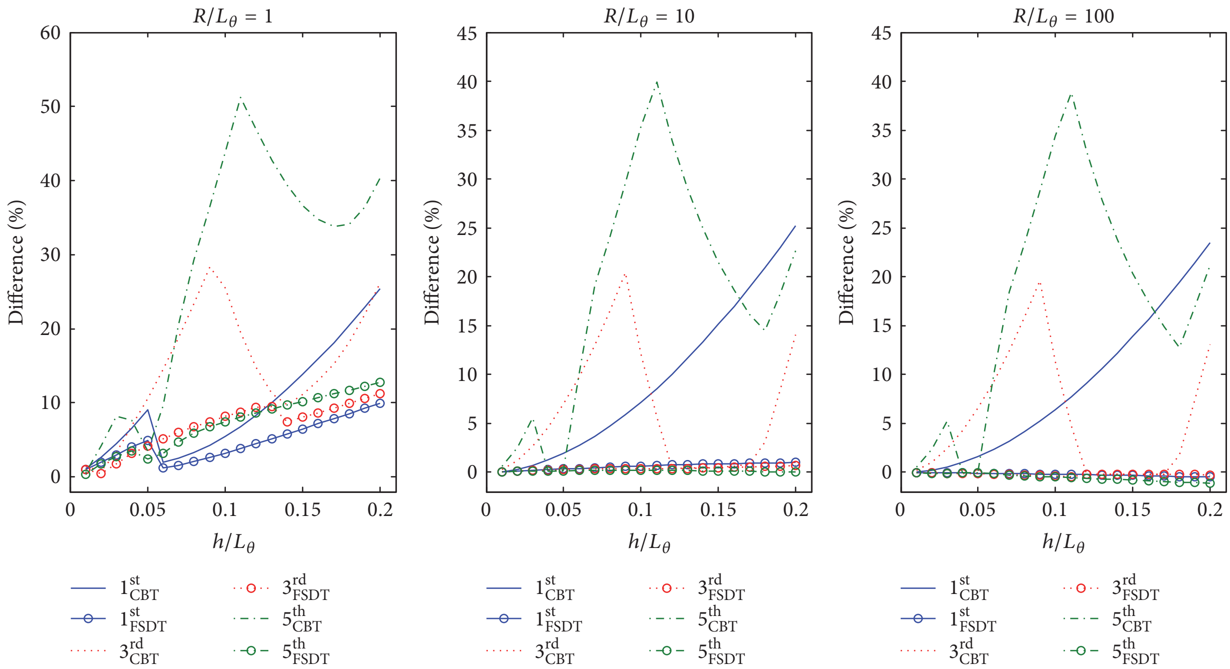

FIGURE 4: Relative deviations between frequency parameters Ω based on the CBT/FSDT theory models to those of 2D theory for circular beams with various thickness ratios (C-C boundary condition).

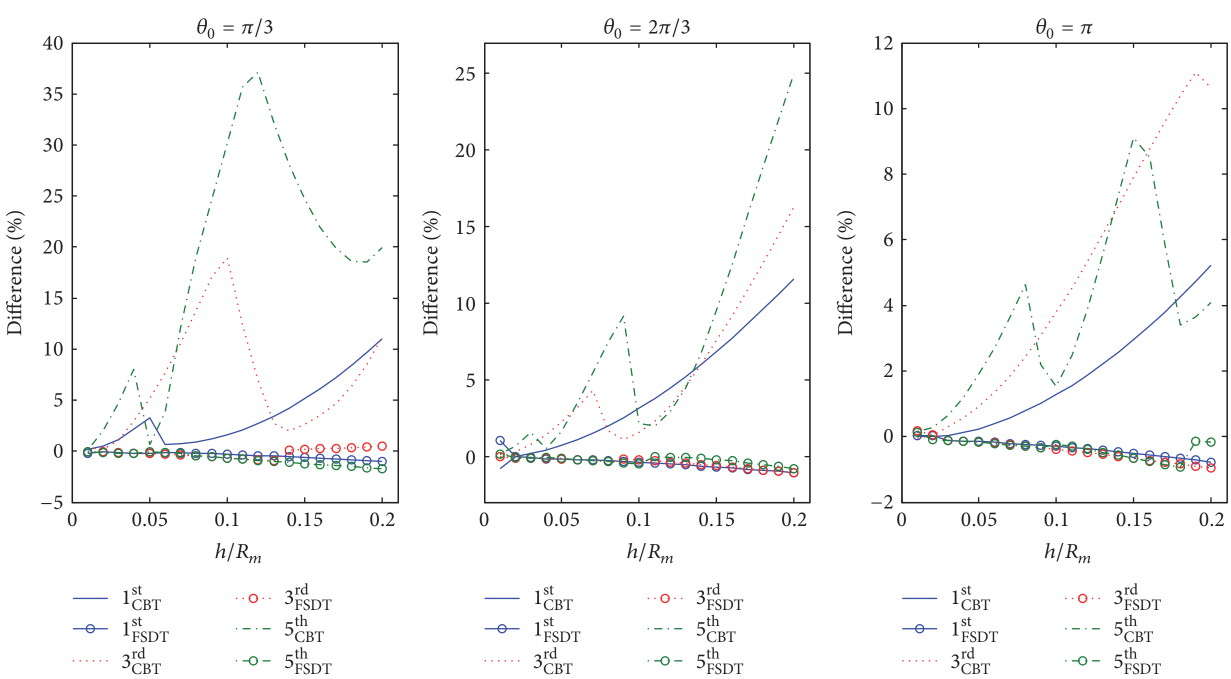

FIGURE 5: Relative deviations between frequency parameters Ω based on the CBT/FSDT theory models to those of 2D theory for circular beams with different thickness-to-radius ratios (C-C boundary condition).

and FSDT results can be as many as 21.6% and 25.3% for the F-F and C-C boundary conditions, respectively. In addition, it is obvious that the transverse shear deformation has greater influence on the higher modes.

Elasticity solutions for circular beams with different geometrical dimensions and several sets of classical boundary conditions are presented in the following presentation. The lowest six frequencies considering three different thickness-to-radius ratios are presented in Table 4 ($\Delta\theta = \pi/2$), where the classical boundary conditions are included. "$N \times J = 17 \times 9$" displacement field is adopted in this study. From the results of Table 4, it becomes clear that the frequency parameters

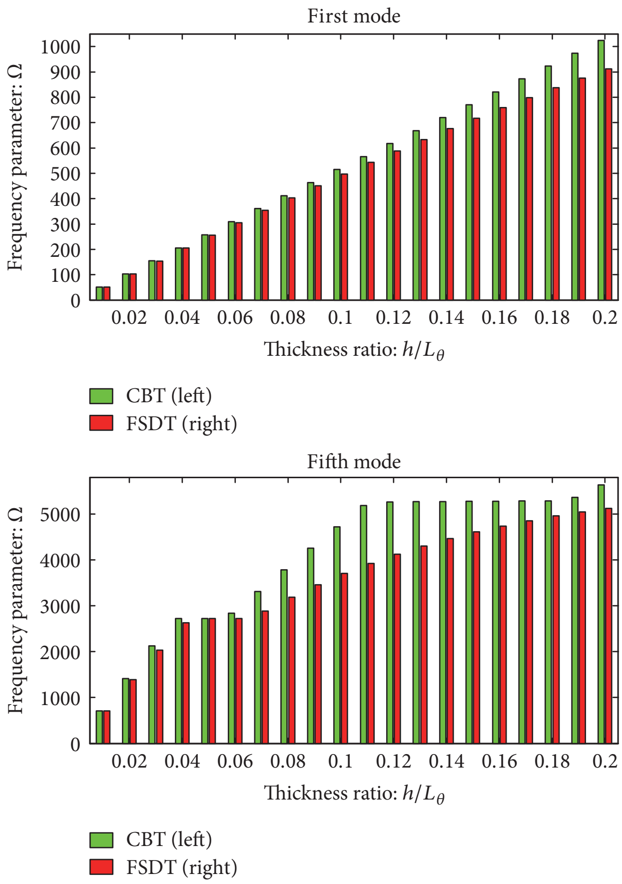

Figure 6: Frequency parameters Ω of circular beams with various thickness ratios based on the CBT and FSDT theory models (F-F boundary condition).

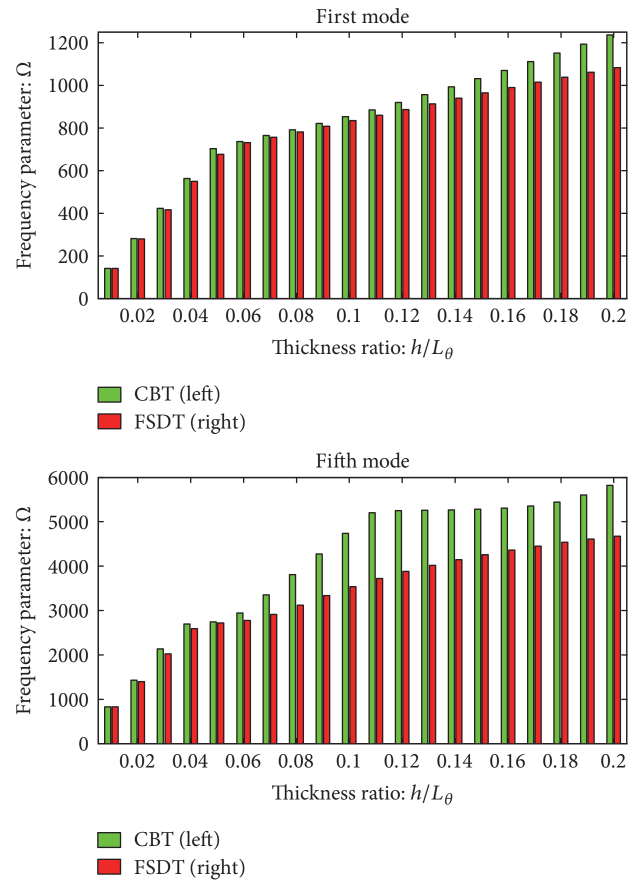

Figure 7: Frequency parameters Ω of circular beams with various thickness ratios based on the CBT and FSDT theory models (C-C boundary condition).

Ω decrease when the thickness of the beams is increased. However, it should be pointed out that the beam's natural frequencies (Hz) are increasing actually because the stiffness of a beam increases generally when its thickness is increased. For the sake of completeness, the first three modal shapes for the beam with C-C boundary conditions are presented in Figure 8. The figure indicates that the modal shapes of thick beams are characterized by complex coupling between the extension, bending, and shearing modes.

The lowest six frequency parameters Ω of the certain circular beams are presented in Table 5 with a variety of classical restraints and span angles. The thickness ratio (h/R_m) of the beams is assumed to be constant as $h/R_m = 0.1, 20$. Meanwhile, the span angle $\Delta\theta$ is taken as $\Delta\theta = \pi/3, 2\pi/3$, and π, respectively. "$N \times J = 20 \times 9$" displacement field is adopted in this study. First of all, it is seen that the circular beams with C-C boundary conditions have highest frequency parameters among all boundary cases. The frequency parameters of the beam decrease when the span angle increases because when the span angle increases, the flexibility of the beam increases synchronously. Figure 9 gives the three lowest mode shapes for the circular beam of Table 6 with FC restraint. The figure reveals that the change in the span angle can directly affect the mode shapes of the beam. The modes of the beam are noted to be determined by bending, shear, and normal deformation, which could not be determined by the CBT and FSDT theory models.

Figure 10 shows the deviations between the first, third, and fifth frequency parameters Ω based on the CBT/FSDT theory models and those of the current 2D formulation for circular beams for various values of thickness-to-radius ratios and restraint rigidities. The beams ($L_\theta = 1$) are supposed to be clamped at one end ($\theta = \theta_0$) and elastically supported at the other end with stiffness rigidity $k_u^1 = k_w^1 = \eta$ (where $\eta/D \in [10^{-2}, 10^8]$, $D = Eh^3/12$). "$N \times J = 17 \times 9$" displacement field is adopted in this study. From the figure, it is obvious that the effects of the transverse normal and shear deformation have a great influence on the frequencies of the beam when subjected to elastic boundary conditions. According to Figure 10, we can see that the errors of the CBT and FSDT are acceptable when the restraint rigidity η/D is smaller than 10^{-1}. However, the error increases sharply when it is increased from 10^{-1} to 10^5. Then, the error decreases and remains the same when η/D tends to be infinity. The error of the CBT/FSDT can be as much as 180%, 120%, and 85% for the worst case in each study.

Figures 11–13 show similar study for circular beams with different type of elastic boundary restraints. The following

Table 4: The lowest six frequency parameters Ω of classically restrained circular beams with various thickness ratios ($R_m = 1$ m, $\Delta\theta = \pi/2$).

h/R_m	Mode	Boundary condition									
		F-F	F-S1	F-S2	F-C	S1-S1	S1-S2	S1-C	S2-S2	S2-C	C-C
0.05	1	8.3653	5.2974	1.8360	1.4976	2.6801	7.5652	4.3680	2.6800	9.5587	22.270
	2	23.694	18.869	11.065	7.1854	14.464	23.307	17.702	14.464	26.891	39.349
	3	46.884	40.247	28.619	22.477	34.040	46.609	38.807	34.039	50.676	66.753
	4	77.238	68.895	53.693	45.339	60.960	77.028	66.582	60.959	66.953	74.701
	5	114.23	104.30	85.785	74.297	94.751	97.943	92.155	69.297	86.221	114.39
	6	154.82	145.91	97.943	94.711	134.88	114.06	106.77	94.749	123.04	143.50
0.1	1	8.2897	5.2643	1.8326	1.4942	2.6707	7.4945	4.3126	2.6706	9.2748	21.246
	2	23.048	18.453	10.919	7.0603	14.213	22.672	17.053	14.213	24.596	27.624
	3	44.492	38.450	27.682	21.456	32.728	44.232	35.608	32.727	34.057	46.328
	4	71.197	63.988	48.914	40.384	57.039	48.917	47.535	34.672	50.034	64.343
	5	77.261	77.261	50.605	49.486	77.259	71.006	63.829	57.038	73.445	79.316
	6	102.04	93.921	78.471	70.567	86.002	101.899	92.113	77.257	80.161	98.509
0.2	1	8.0147	5.1403	1.8195	1.4802	2.6343	7.2362	4.1083	2.6343	8.2708	16.029
	2	20.994	17.077	10.404	6.6156	13.354	20.658	14.846	13.354	16.094	18.192
	3	37.663	33.367	24.305	17.818	28.877	24.349	23.209	17.384	24.260	35.875
	4	38.678	38.337	24.870	24.700	38.320	37.789	32.799	28.876	36.821	36.990
	5	57.082	52.145	42.532	36.793	47.221	54.074	49.629	38.319	42.107	53.898
	6	70.432	70.314	54.084	53.013	67.144	57.039	54.498	47.220	59.788	68.390

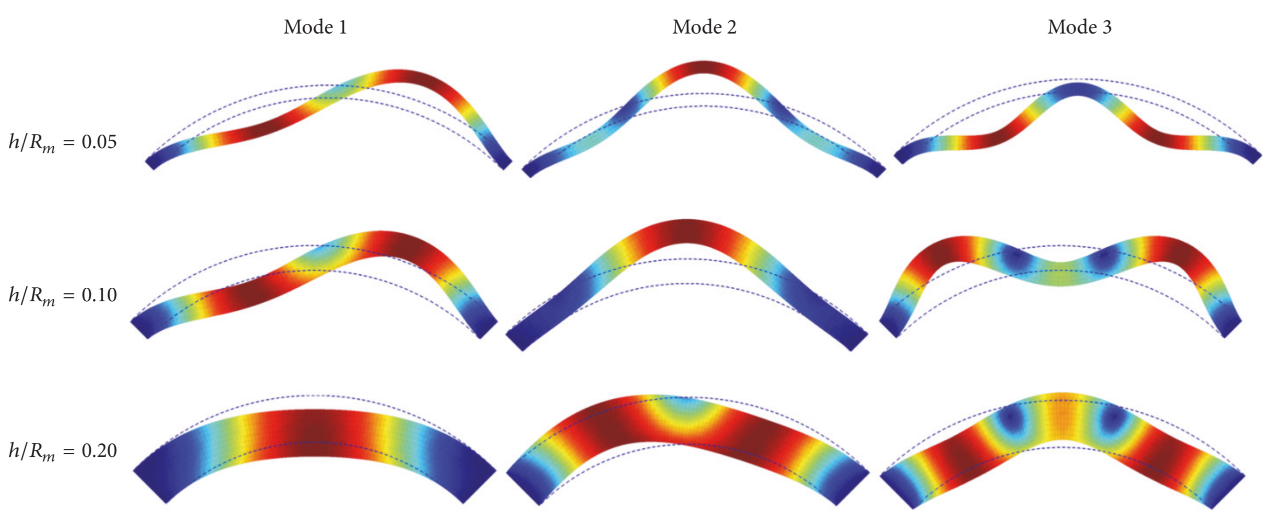

Figure 8: Modal shapes relative to the C-C circular curved beams of Table 4.

geometric parameters are used: $R_m = 1, h/R_m = 0.2$. The beam is clamped at the end of $\theta = \theta_0$ and elastically restrained at the other end. The following three types of elastic supports are considered in the study: axially elastic restraint ($k_u^1 = \eta,\ k_w^1 = 0$), transversely elastic restraint ($k_u^1 = 0,\ k_w^1 = \eta$), and elastic restraint in both directions ($k_u^1 = k_w^1 = \eta$). The changes of the relative deviations between frequency parameters Ω based on the CBT/FSDT theory models and those of the current 2D formulation with respect to elastic rigidity η/D are the same as Figure 10.

Finally, Table 6 displays the lowest three nondimensional frequencies Ω for circular beams with a variety of geometric constants and restrained rigidities. The elastic boundary conditions studied in the table are the same as those of Figures 11–13. The geometrical dimensions used in the calculation are $R_m = 1$ m, $\theta_0 = \pi/2$. "$N \times J = 17 \times 9$" displacement field is adopted in this study. The table reveals that the frequencies of the beam will increase when the rigidity of the restraint increases. This is because when the restraint rigidity increases, the stiffness of the beam increases synchronously while the mass remains unchanged. Table 7 shows similar studies for the beams with different span angles. The geometrical parameters and material properties used in the calculation are $R_m = 1$ m, $h/R_m = 0.1$. These results can

Table 5: The lowest six frequency parameters Ω of classically restrained circular beams with various span angles (R_m = 1 m, h/R_m = 0.1).

$\Delta\theta$	Mode	Boundary condition									
		F-F	F-S1	F-S2	F-C	S1-S1	S1-S2	S1-C	S2-S2	S2-C	C-C
$\pi/3$	1	19.088	12.761	4.4804	3.2579	7.4946	1.0378	11.416	7.4943	20.441	34.046
	2	50.820	41.432	25.315	17.105	32.728	18.234	38.524	32.727	34.047	47.270
	3	94.059	82.289	60.572	46.643	71.007	50.481	60.019	34.672	59.680	90.478
	4	109.23	109.21	62.328	62.105	109.21	62.312	81.544	71.005	101.17	106.39
	5	144.99	131.64	106.10	92.330	118.59	93.844	128.08	109.20	110.73	139.31
	6	200.96	186.60	158.38	140.84	172.44	144.88	158.76	118.58	154.51	189.04
$2\pi/3$	1	4.4805	2.6710	0.9739	0.8749	1.0378	0.2623	1.9658	1.0378	4.7592	11.419
	2	12.761	10.031	5.7637	3.6195	7.4946	3.6888	9.0668	7.4945	14.121	20.445
	3	25.315	21.674	15.360	11.728	18.234	12.365	20.381	18.234	26.580	34.049
	4	41.432	36.989	28.906	23.886	32.728	25.042	34.259	32.727	34.065	38.533
	5	60.573	55.456	43.262	37.328	50.482	41.228	42.524	34.672	45.344	59.694
	6	62.330	62.315	45.861	44.506	62.313	43.263	55.402	50.481	59.944	60.023
π	1	1.8327	0.9507	0.4372	0.4349	2.6707	1.0378	3.3476	2.6706	1.5851	4.3142
	2	5.2643	3.9432	2.1308	1.3692	7.4946	4.8346	8.4943	7.4945	5.6604	9.2781
	3	10.919	9.1645	6.3020	4.6433	14.213	10.627	15.497	14.213	11.769	17.059
	4	18.453	16.288	12.501	10.245	22.673	18.234	24.055	22.672	19.579	24.603
	5	27.683	25.134	20.505	17.608	32.728	27.510	33.194	32.728	28.529	34.059
	6	38.450	35.548	30.155	26.470	44.232	38.308	38.551	34.673	34.072	35.618

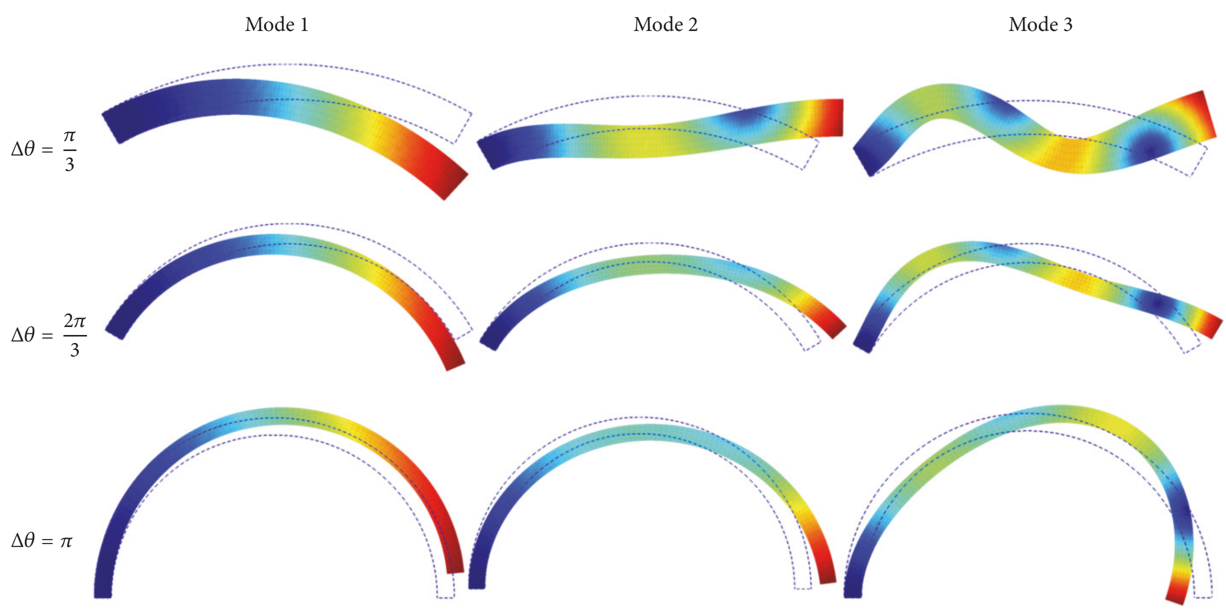

Figure 9: Modal shapes relative to the F-C circular curved beams of Table 5.

be used to verify new 1D refined beam theories for further studies.

4. Conclusions

This paper proposes an accurate modified Fourier series-based sampling surface approach for the analytical evaluation of the vibration characteristics of thick curved beams. The approach is valid for arbitrary thickness configuration and maintains its simplicity and uniform in any type of boundary conditions (i.e., classical boundary condition, elastic support, or their combination). The theoretical models of the beams are based on the 2D theory of elasticity including the effects of both transverse shear and normal deformations. Under the current framework, the transverse beam domain is discretized by a set of nonequally spaced sampling surfaces and the displacement components coinciding with these surfaces are mathematically described as an set of modified Fourier

Table 6: Frequency parameters Ω for elastically supported circular beams with different thickness ratios and restraint rigidities (R_m = 1 m, $\theta_0 = \pi/2$).

h/R_m	η/D	$ku=\eta,\ kw=0$			$ku=0,\ kw=\eta$			$ku=kw=\eta$		
		1	2	3	1	2	3	1	2	3
0.01	10^0	1.5013	7.2263	22.817	1.5040	7.2283	22.818	1.5066	7.2283	22.818
	10^1	1.5249	7.2266	22.817	1.5515	7.2464	22.823	1.5770	7.2467	22.823
	10^2	1.7442	7.2296	22.818	1.9406	7.4289	22.877	2.1392	7.4312	22.878
	10^3	3.1816	7.2654	22.825	3.3673	9.2160	23.442	4.4370	9.2166	23.451
	10^4	6.8030	9.5884	22.907	4.2514	15.578	29.613	9.5523	15.677	29.817
	10^5	7.0247	21.852	30.250	4.3720	17.693	38.640	17.584	25.942	40.813
0.05	10^0	1.5109	7.1856	22.477	1.5243	7.1955	22.480	1.5374	7.1957	22.480
	10^1	1.6253	7.1873	22.477	1.7397	7.2863	22.506	1.8517	7.2878	22.507
	10^2	2.4911	7.2050	22.483	2.8562	8.2070	22.780	3.5131	8.2091	22.786
	10^3	6.0299	7.7159	22.538	4.1096	13.588	25.951	7.4008	13.649	26.053
	10^4	7.0667	18.929	23.904	4.3410	17.262	36.620	16.954	18.929	37.704
	10^5	7.7839	22.923	44.333	4.3653	17.659	38.610	18.203	33.998	52.083
0.10	10^0	1.5207	7.0608	21.456	1.5468	7.0804	21.461	1.5725	7.0808	21.462
	10^1	1.7408	7.0650	21.458	1.9337	7.2624	21.514	2.1335	7.2658	21.516
	10^2	3.1733	7.1131	21.481	3.3372	9.0383	22.066	4.4148	9.0427	22.094
	10^3	6.6891	9.3939	21.720	4.1854	15.042	27.958	9.3746	15.112	28.313
	10^4	7.4853	19.902	25.792	4.2996	16.861	34.871	17.240	20.798	37.990
	10^5	8.7622	23.296	32.768	4.3113	17.034	35.536	19.364	26.704	43.372
0.15	10^0	1.5282	6.8657	19.865	1.5660	6.8947	19.872	1.6040	6.8956	19.873
	10^1	1.8473	6.8741	19.872	2.0917	7.1678	19.946	2.3677	7.1741	19.954
	10^2	3.7026	6.9755	19.942	3.5429	9.6553	20.751	4.9852	9.6663	20.838
	10^3	6.7367	10.615	20.652	4.1440	14.969	26.889	10.523	15.059	28.171
	10^4	7.8630	17.816	24.479	4.2159	15.961	28.964	17.085	18.064	36.130
	10^5	8.6753	19.710	26.673	4.2233	16.055	29.097	19.121	19.856	39.345

Table 7: Frequency parameters Ω for elastically supported circular beams with different span angles and restraint rigidities (R_m = 1 m, $h/R_m = 0.1$).

θ_0	η/D	$ku=\eta,\ kw=0$			$ku=0, kw=\eta$			$ku=kw=\eta$		
		1	2	3	1	2	3	1	2	3
$\pi/3$	10^0	3.2671	17.105	46.643	3.3052	17.116	46.646	3.3143	17.117	46.646
	10^1	3.3484	17.110	46.647	3.6978	17.217	46.674	3.7784	17.222	46.679
	10^2	4.0665	17.154	46.688	6.0927	18.272	46.962	6.5964	18.303	47.008
	10^3	8.0451	17.639	47.081	10.265	27.077	50.196	13.084	27.089	50.748
	10^4	15.321	23.449	49.869	11.295	37.199	59.270	23.265	37.875	68.723
	10^5	18.965	31.838	55.957	11.403	38.393	59.956	31.839	42.697	83.774
$2\pi/3$	10^0	0.9258	3.6197	11.729	0.9197	3.6507	11.737	0.9683	3.6508	11.737
	10^1	1.2960	3.6210	11.731	1.2006	3.9285	11.815	1.5359	3.9290	11.818
	10^2	3.1142	3.6536	11.753	1.7696	5.9362	12.680	3.3494	5.9983	12.716
	10^3	3.6599	9.1322	12.165	1.9434	8.6156	18.070	7.8507	9.3882	18.576
	10^4	3.9841	12.050	23.150	1.9635	9.0227	20.175	9.2396	17.386	26.000
	10^5	4.5641	13.485	25.680	1.9656	9.0622	20.360	10.492	19.461	32.929
π	10^0	0.5264	1.3719	4.6438	0.4487	1.4211	4.6595	0.5367	1.4241	4.6599
	10^1	1.0030	1.4177	4.6480	0.5063	1.8014	4.8097	1.0033	1.8520	4.8159
	10^2	1.3161	3.0900	4.7182	0.5555	2.9075	6.2241	2.3074	3.3600	6.3712
	10^3	1.3396	4.5807	9.8024	0.5642	3.3007	8.2147	3.1616	6.9331	9.9866
	10^4	1.4308	4.9059	10.622	0.5651	3.3429	8.4675	3.4291	8.1148	15.259
	10^5	1.5524	5.4708	11.429	0.5652	3.3471	8.4916	4.0046	8.7902	16.261

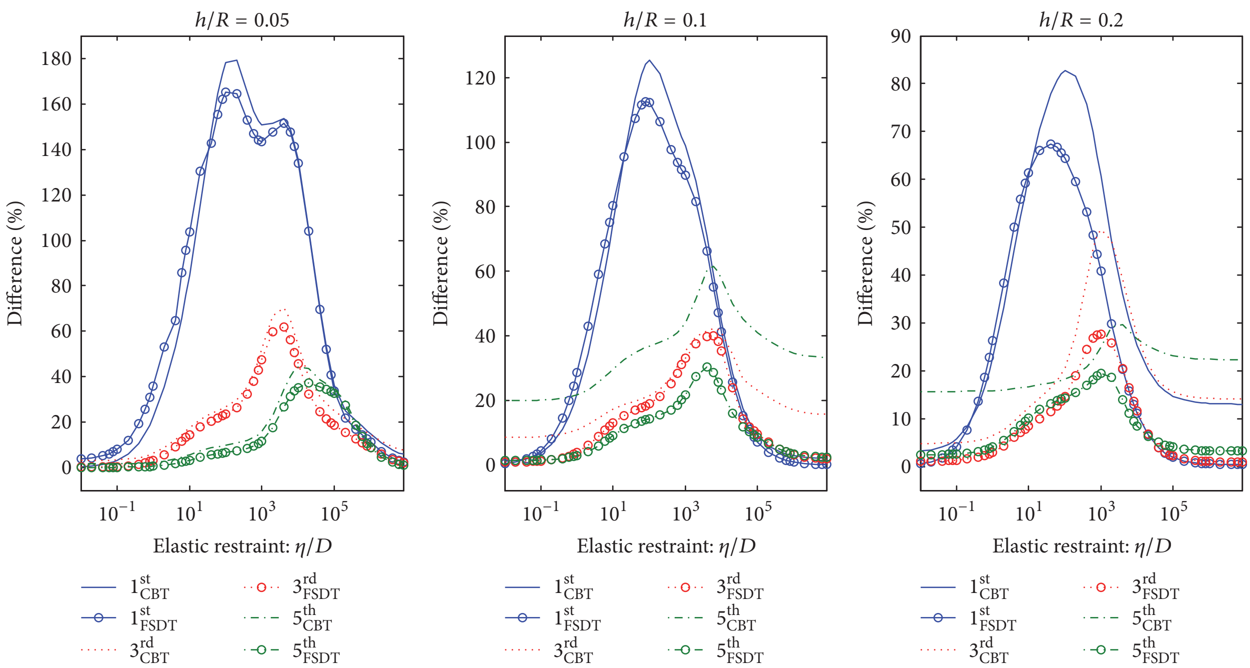

FIGURE 10: Relative deviations between frequency parameters Ω based on the CBT/FSDT theory models to those of 2D theory for elastically restrained circular beams with different restraint rigidities ($\theta = \theta_0$: clamped; $\theta = \theta_1$: $ku = kw = \eta$).

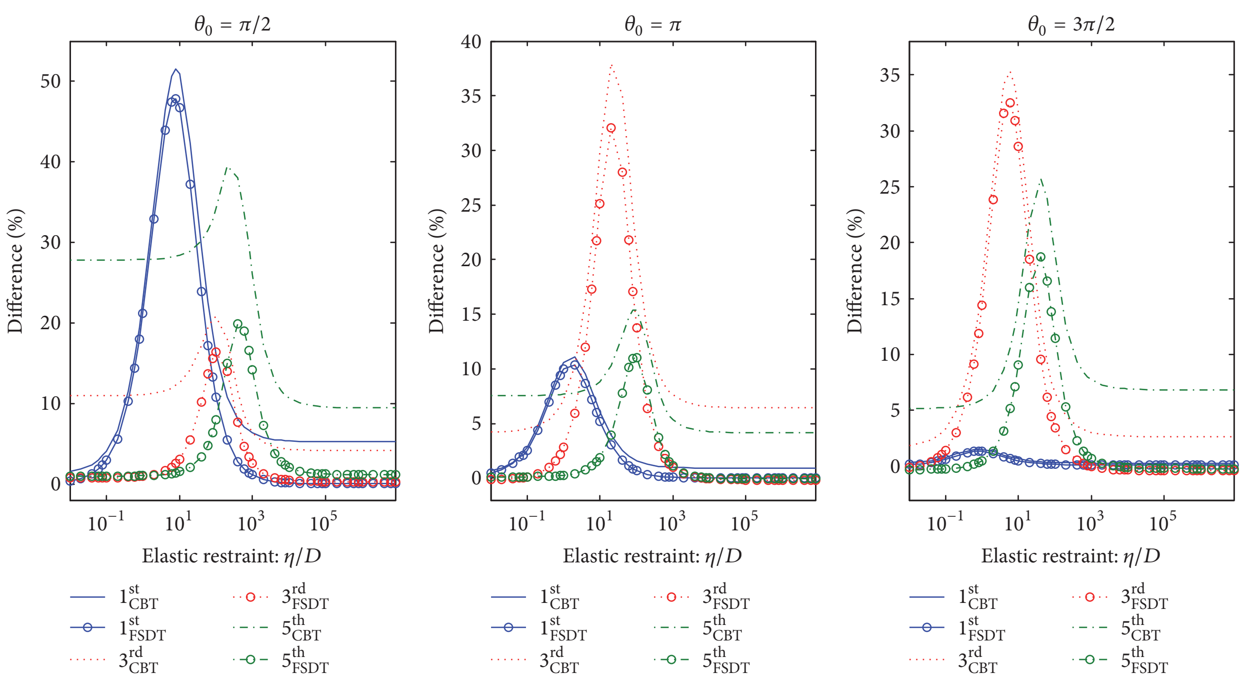

FIGURE 11: Relative deviations between frequency parameters Ω based on the CBT/FSDT theory models to those of 2D theory for elastically restrained circular beams with different restraint rigidities ($\theta = \theta_0$: clamped; $\theta = \theta_1$: $k_u^1 = \eta$, $k_w^1 = 0$).

series including the certain auxiliary terms which are used to form a mathematically complete set and guarantee the results convergent to the exact solutions. The governing equations of the beams are derived and numerically solved using a modified variational principle by the use of the penalty technique as well as Lagrange multipliers. Elasticity solutions including transverse shear and normal effects are compared with the corresponding one-dimensional results in terms of the classical and first-order shear deformation theories. The influences of transverse normal and shear deformation on

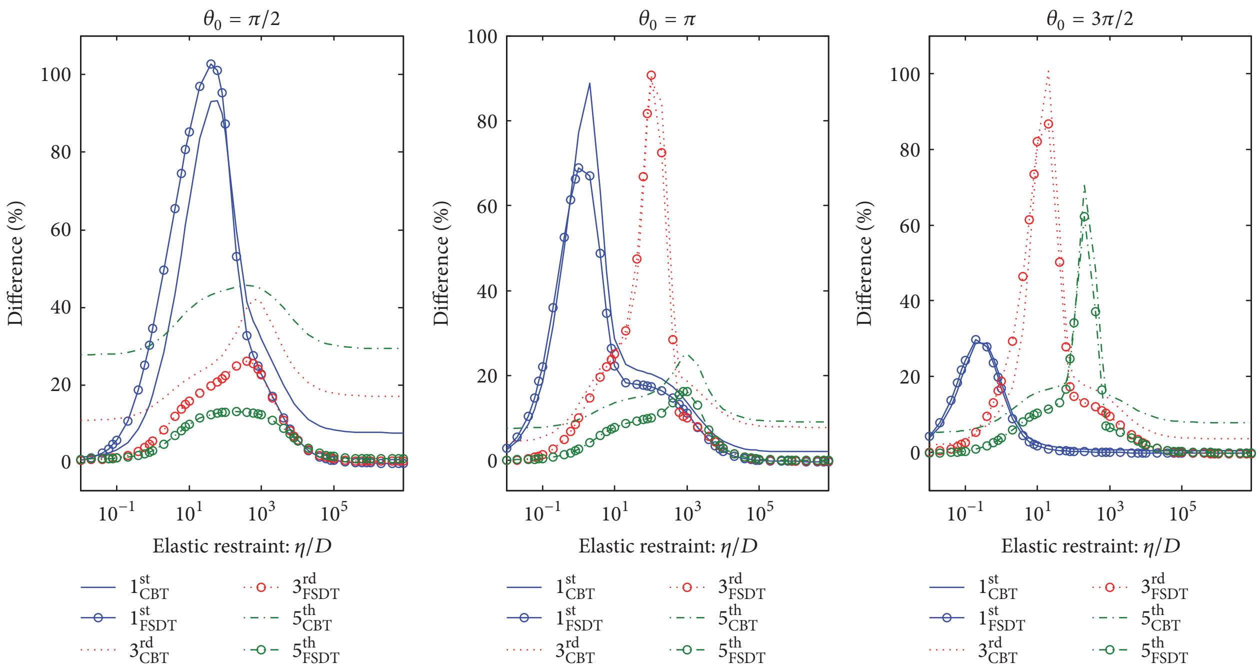

FIGURE 12: Relative deviations between frequency parameters Ω based on the CBT/FSDT theory models to those of 2D theory for elastically restrained circular beams with different restraint rigidities ($\theta = \theta_0$: clamped; $\theta = \theta_1$: $k_u^1 = 0$, $k_w^1 = \eta$).

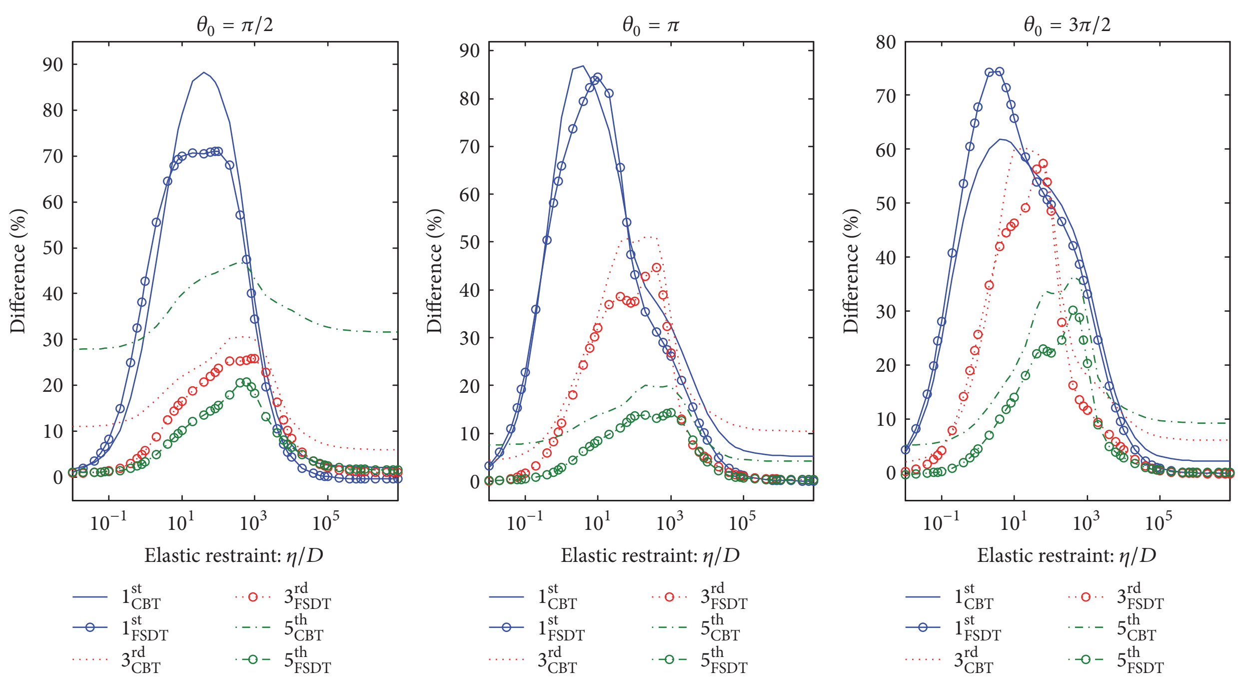

FIGURE 13: Relative deviations between frequency parameters Ω based on the CBT/FSDT theory models to those of 2D theory for elastically restrained circular beams with different restraint rigidities ($\theta = \theta_0$: clamped; $\theta = \theta_1$: $k_u^1 = k_w^1 = \eta$).

the vibration characteristics are systematically evaluated. The results show that the proposed method is applicable for thick circular beams with arbitrary boundary conditions.

Conflicts of Interest

The authors declare that there are no conflicts of interest regarding the publication of this paper.

References

[1] M. S. Qatu, *Vibration of Laminated Shells and Plates*, Elsevier Science, 2004.

[2] E. Viola, M. Dilena, and F. Tornabene, “Analytical and numerical results for vibration analysis of multi-stepped and multi-damaged circular arches,” *Journal of Sound and Vibration*, vol. 299, no. 1-2, pp. 143–163, 2007.

[3] P. Malekzadeh, M. M. Atashi, and G. Karami, "In-plane free vibration of functionally graded circular arches with temperature-dependent properties under thermal environment," *Journal of Sound and Vibration*, vol. 326, no. 3-5, pp. 837–851, 2009.

[4] M. S. Qatu, "Theories and analyses of thin and moderately thick laminated composite curved beams," *International Journal of Solids and Structures*, vol. 30, no. 20, pp. 2743–2756, 1993.

[5] T. Ye, G. Jin, X. Ye, and X. Wang, "A series solution for the vibrations of composite laminated deep curved beams with general boundaries," *Composite Structures*, vol. 127, pp. 450–465, 2015.

[6] Y. Qu, Y. Chen, X. Long, H. Hua, and G. Meng, "A variational method for free vibration analysis of joined cylindrical-conical shells," *Journal of Vibration and Control*, vol. 19, no. 16, pp. 2319–2334, 2013.

[7] M. Hajianmaleki and M. S. Qatu, "Static and vibration analyses of thick, generally laminated deep curved beams with different boundary conditions," *Composites Part B: Engineering*, vol. 43, no. 4, pp. 1767–1775, 2012.

[8] L. Jun, S. Rongying, H. Hongxing, and J. Xianding, "Coupled bending and torsional vibration of axially loaded Bernoulli-Euler beams including warping effects," *Applied Acoustics*, vol. 65, no. 2, pp. 153–170, 2004.

[9] X.-F. Li, Y.-A. Kang, and J.-X. Wu, "Exact frequency equations of free vibration of exponentially functionally graded beams," *Applied Acoustics*, vol. 74, no. 3, pp. 413–420, 2013.

[10] K. Suddoung, J. Charoensuk, and N. Wattanasakulpong, "Vibration response of stepped FGM beams with elastically end constraints using differential transformation method," *Applied Acoustics*, vol. 77, pp. 20–28, 2014.

[11] M. H. Toorani and A. A. Lakis, "General equations of anisotropic plates and shells including transverse shear deformations, rotary inertia and initial curvature effects," *Journal of Sound and Vibration*, vol. 237, no. 4, pp. 561–615, 2000.

[12] E. Carrera, "Theories and finite elements for multilayered, anisotropic, composite plates and shells," *Archives of Computational Methods in Engineering. State of the Art Reviews*, vol. 9, no. 2, pp. 87–140, 2002.

[13] E. Carrera, "Theories and finite elements for multilayered plates and shells: a unified compact formulation with numerical assessment and benchmarking," *Archives of Computational Methods in Engineering*, vol. 10, no. 3, pp. 215–296, 2003.

[14] W. Q. Chen, C. F. Lü, and Z. G. Bian, "A mixed method for bending and free vibration of beams resting on a Pasternak elastic foundation," *Applied Mathematical Modelling*, vol. 28, no. 10, pp. 877–890, 2004.

[15] J. Ying, C. F. Lü, and W. Q. Chen, "Two-dimensional elasticity solutions for functionally graded beams resting on elastic foundations," *Composite Structures*, vol. 84, no. 3, pp. 209–219, 2008.

[16] S. M. Hasheminejad and A. Rafsanjani, "Two-dimensional elasticity solution for transient response of simply supported beams under moving loads," *Acta Mechanica*, vol. 217, no. 3-4, pp. 205–218, 2011.

[17] Y. Xu and D. Zhou, "Two-dimensional thermoelastic analysis of beams with variable thickness subjected to thermo-mechanical loads," *Applied Mathematical Modelling. Simulation and Computation for Engineering and Environmental Systems*, vol. 36, no. 12, pp. 5818–5829, 2012.

[18] Y. Xu and D. Zhou, "Elasticity solution of multi-span beams with variable thickness under static loads," *Applied Mathematical Modelling. Simulation and Computation for Engineering and Environmental Systems*, vol. 33, no. 7, pp. 2951–2966, 2009.

[19] A. M. Zenkour, M. N. M. Allam, and M. Sobhy, "Effect of transverse normal and shear deformation on a fiber-reinforced viscoelastic beam resting on two-parameter elastic foundations," *International Journal of Applied Mechanics*, vol. 2, no. 1, pp. 87–115, 2010.

[20] P. Malekzadeh and G. Karami, "A mixed differential quadrature and finite element free vibration and buckling analysis of thick beams on two-parameter elastic foundations," *Applied Mathematical Modelling*, vol. 32, no. 7, pp. 1381–1394, 2008.

[21] A. Rosen, "Structural and dynamic behavior of pretwisted rods and beams," *Applied Mechanics Reviews*, vol. 44, no. 12, pp. 483–515, 1991.

[22] P. Chidamparam and A. W. Leissa, "Vibrations of planar curved beams, rings, and arches," *Applied Mechanics Reviews*, vol. 46, no. 9, pp. 467–483, 1993.

[23] D. H. Hodges, *Nonlinear Composite Beam Theory*, American Institute of Aeronautics and Astronautics, Reston ,VA, USA, 2006.

[24] M. Hajianmaleki and M. S. Qatu, "Vibrations of straight and curved composite beams: A review," *Composite Structures*, vol. 100, pp. 218–232, 2013.

[25] F. Tornabene, N. Fantuzzi, M. Bacciocchi, and E. Viola, "Accurate inter-laminar recovery for plates and doubly-curved shells with variable radii of curvature using layer-wise theories," *Composite Structures*, vol. 124, pp. 368–393, 2015.

[26] E. Carrera, S. Brischetto, M. Cinefra, and M. Soave, "Effects of thickness stretching in functionally graded plates and shells," *Composites Part B: Engineering*, vol. 42, no. 2, pp. 123–133, 2011.

[27] W. T. Koiter, "A consistent first approximation in the general theory of thin elastic shells," in *Proceedings of first symposium on the theory of thin elastic shells*, North-Holland, Amsterdam, 1960.

[28] T. Ye and G. Jin, "Elasticity solution for vibration of generally laminated beams by a modified Fourier expansion-based sampling surface method," *Computers and Structures*, vol. 167, pp. 115–130, 2016.

[29] W. L. Li, "Free vibrations of beams with general boundary conditions," *Journal of Sound and Vibration*, vol. 237, no. 4, pp. 709–725, 2000.

[30] G. M. Kulikov, S. V. Plotnikova, M. G. Kulikov, and P. V. Monastyrev, "Three-dimensional vibration analysis of layered and functionally graded plates through sampling surfaces formulation," *Composite Structures*, vol. 152, pp. 349–361, 2016.

[31] G. M. Kulikov and S. V. Plotnikova, "Three-Dimensional Solution of the Free Vibration Problem for Metal-Ceramic Shells Using the Method of Sampling Surfaces," *Mechanics of Composite Materials*, vol. 53, no. 1, pp. 31–44, 2017.

[32] G. Jin, T. Ye, and Z. Su, "Elasticity solution for vibration of 2-D curved beams with variable curvatures using a spectral-sampling surface method," *International Journal for Numerical Methods in Engineering*, vol. 111, no. 11, pp. 1075–1100, 2017.

[33] G. M. Kulikov, "Refined global approximation theory of multilayered plates and shells," *Journal of Engineering Mechanics*, vol. 127, no. 2, pp. 119–125, 2001.

[34] G. M. Kulikov and E. Carrera, "Finite deformation higher-order shell models and rigid-body motions," *International Journal of Solids and Structures*, vol. 45, no. 11-12, pp. 3153–3172, 2008.

[35] G. M. Kulikov and S. V. Plotnikova, "Exact 3D stress analysis of laminated composite plates by sampling surfaces method," *Composite Structures*, vol. 94, no. 12, pp. 3654–3663, 2012.

[36] W. L. Li, "Comparison of fourier sine and cosine series expansions for beams with arbitrary boundary conditions," *Journal of Sound and Vibration*, vol. 255, no. 1, pp. 185–194, 2003.

[37] G. Jin, T. Ye, and S. Shi, "Three-dimensional vibration analysis of isotropic and orthotropic open shells and plates with arbitrary boundary conditions," *Shock and Vibration*, vol. 2015, Article ID 896204, 29 pages, 2015.

[38] T. Ye, G. Jin, and Y. Zhang, "Vibrations of composite laminated doubly-curved shells of revolution with elastic restraints including shear deformation, rotary inertia and initial curvature," *Composite Structures*, vol. 133, pp. 202–225, 2015.

[39] G. Jin, T. Ye, X. Wang, and X. Miao, "A unified solution for the vibration analysis of FGM doubly-curved shells of revolution with arbitrary boundary conditions," *Composites Part B: Engineering*, vol. 89, pp. 230–252, 2016.

[40] Z. Su, G. Jin, and T. Ye, "Vibration analysis and transient response of a functionally graded piezoelectric curved beam with general boundary conditions," *Smart Materials and Structures*, vol. 25, no. 6, Article ID 065003, 2016.

[41] T. Ye, G. Jin, and Z. Su, "Three-dimensional vibration analysis of laminated functionally graded spherical shells with general boundary conditions," *Composite Structures*, vol. 116, no. 1, pp. 571–588, 2014.

[42] T. Ye, G. Jin, and Z. Su, "Three-dimensional vibration analysis of functionally graded sandwich deep open spherical and cylindrical shells with general restraints," *Journal of Vibration and Control*, vol. 22, no. 15, pp. 3326–3354, 2016.

[43] G. Jin, T. Ye, X. Ma, Y. Chen, Z. Su, and X. Xie, "A unified approach for the vibration analysis of moderately thick composite laminated cylindrical shells with arbitrary boundary conditions," *International Journal of Mechanical Sciences*, vol. 75, pp. 357–376, 2013.

[44] Z. Su, G. Jin, Y. Wang, and X. Ye, "A general Fourier formulation for vibration analysis of functionally graded sandwich beams with arbitrary boundary condition and resting on elastic foundations," *Acta Mechanica*, vol. 227, no. 5, pp. 1493–1514, 2016.

[45] G. Jin, T. Ye, X. Jia, and S. Gao, "A general Fourier solution for the vibration analysis of composite laminated structure elements of revolution with general elastic restraints," *Composite Structures*, vol. 109, no. 1, pp. 150–168, 2014.

[46] Y. Qu, Y. Chen, X. Long, H. Hua, and G. Meng, "A modified variational approach for vibration analysis of ring-stiffened conical-cylindrical shell combinations," *European Journal of Mechanics. A. Solids*, vol. 37, pp. 200–215, 2013.

[47] Y. Qu, X. Long, H. Li, and G. Meng, "A variational formulation for dynamic analysis of composite laminated beams based on a general higher-order shear deformation theory," *Composite Structures*, vol. 102, pp. 175–192, 2013.

[48] T. Ye, G. Jin, and Z. Su, "Three-dimensional vibration analysis of sandwich and multilayered plates with general ply stacking sequences by a spectral-sampling surface method," *Composite Structures*, vol. 176, pp. 1124–1142, 2017.

[49] S. Ilanko, "Penalty methods for finding eigenvalues of continuous systems: Emerging challenges and opportunities," *Computers and Structures*, vol. 104-105, pp. 50–54, 2012.